REPORT DOCUMENTATION PAGE

Form Approved
OMB No. 074-0188

1. AGENCY USE ONLY (Leave blank)	2. REPORT DATE	3. REPORT TYPE AND DATES COVERED
	Apr. 1- Jun. 30, 1995	Quarterly report, April 1- June 30, 1995

4. TITLE AND SUBTITLE
Kinetics of Supercritical Water Oxidation

5. FUNDING NUMBERS
N/A

6. AUTHOR(S)
Steven F. Rice

7. PERFORMING ORGANIZATION NAME(S) AND ADDRESS(ES)

Sandia National Laboratories
Combustion Research Facility

MIT

Princeton University

8. PERFORMING ORGANIZATION REPORT NUMBER
N/A

9. SPONSORING / MONITORING AGENCY NAME(S) AND ADDRESS(ES)
SERDP
901 North Stuart St. Suite 303
Arlington, VA 22203

10. SPONSORING / MONITORING AGENCY REPORT NUMBER

Case 8610.000

11. SUPPLEMENTARY NOTES
Prepared by Sandia National Laboratories, Combustion Research Facility, Case 8610.000. This work was supported in part by SERDP. The United States Government has a royalty-free license throughout the world in all copyrightable material contained herein. All other rights are reserved by the copyright owner.

12a. DISTRIBUTION / AVAILABILITY STATEMENT
Approved for public release: distribution is unlimited

12b. DISTRIBUTION CODE
A

13. ABSTRACT ***(Maximum 200 Words)***

This project consists of experiments and theoretical modeling designed to improve our understanding of the detailed chemical kinetics of supercritical water oxidation (SCWO) processes. The objective of the three year project is to develop working models that accurately predict the oxidation rates and mechanisms for a variety of key organic species over the range of temperatures and pressures important for industrial applications. Our examination of reaction kinetics in supercritical water undertakes *in situ* measurements of reactants, intermediates, and products using optical spectroscopic techniques, primarily Raman spectroscopy. Our focus is to measure the primary oxidation steps that occur in the oxidation of methanol, phenol, methylene chloride, and some simple organic compounds containing nitro groups with a special emphasis on identifying reaction steps that involve hydroxyl radical and hydrogen peroxide.

14. SUBJECT TERMS
supercritical water oxidation (SCWO), optical spectroscopic techniques, Raman spectroscopy, SERDP

15. NUMBER OF PAGES
23

16. PRICE CODE
N/A

17. SECURITY CLASSIFICATION OF REPORT	18. SECURITY CLASSIFICATION OF THIS PAGE	19. SECURITY CLASSIFICATION OF ABSTRACT	20. LIMITATION OF ABSTRACT
unclass	unclass	unclass	UL

Kinetics of Supercritical Water Oxidation

SERDP Compliance Technical Thrust Area

Quarterly Report

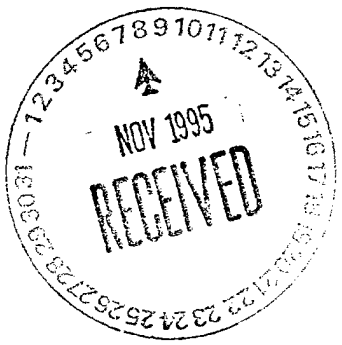

Sandia National Laboratories
Combustion Research Facility
Case 8610.000

Principal Investigator: Steven F. Rice, SNL

Project Associates, SNL: Richard R. Steeper, Thomas B. Hunter, Russell G. Hanush, Jason D. Aiken, Åsa Karlegärd

Research Contractors: Jefferson W. Tester, MIT
Kenneth Brezinsky, Princeton University

Project Manager: Donald R. Hardesty

Reporting Period: April 1 - June 30, 1995

Project description:
This project consists of experiments and theoretical modeling designed to improve our understanding of the detailed chemical kinetics of supercritical water oxidation (SCWO) processes. The objective of the three year project is to develop working models that accurately predict the oxidation rates and mechanisms for a variety of key organic species over the range of temperatures and pressures important for industrial applications. Our examination of reaction kinetics in supercritical water undertakes *in situ* measurements of reactants, intermediates, and products using optical spectroscopic techniques, primarily Raman spectroscopy. Our focus is to measure the primary oxidation steps that occur in the oxidation of methanol, phenol, methylene chloride, and some simple organic compounds containing nitro groups with a special emphasis on identifying reaction steps that involve hydroxyl radical and hydrogen peroxide.

The work conducted here continues the experimental approach from our previous SERDP-funded project by extending measurements on key oxidant species and expanding the variety of experimental methods, primarily optical in nature, that can be used to examine reactions at SCWO conditions. Direct support will be sent to the project collaborators at MIT and Princeton who will contribute to the model development for the halogenated systems and phenol. In general, these researchers will examine these processes using more conventional sample and quench

methods. These experiments all focus on determining the primary oxidation steps that involve the OH and HO_2 radicals, generating data which will be used to evaluate and refine SCWO reaction kinetic schemes. The primary technical difficulty in this stage of the project will be recasting the 1100 °C models for these simple molecules to 400-600 °C emphasizing the role of the HO_2 radical.

Executive Summary of Progress this Period

Programmatic

Several important programmatic milestones were accomplished this quarter. The most critical of these is the successful placement of both research sub-contracts with Prof. J. W. Tester, Dept. of Chemical Engineering, MIT and Dr. K. Brezinsky, Mechanical and Aerospace Engineering Department, Princeton University. The project at MIT will focus on the oxidation and hydrolysis of halogenated species in supercritical water. The project at Princeton is designed to provide new information of pyrolysis and oxidation of phenol and anisole, two simple aromatic species, in the presence of water vapor. In addition, the Execution Plan was written and submitted for the SERDP FY95 funding for this project of $300K and the transfer of funds to the Sandia case is in progress. This project was chosen to be represented in the Compliance TTA session at the First Annual SERDP Symposium in April. The project's progress was also presented to the SERDP Executive committee at the FY95 In Progress Review in May.

Methane oxidation

Work this quarter focused on interpretation of the methane oxidation results and the preparation of a paper. Part of the work presented in Steeper's thesis was supported by SERDP. Results and analysis of the oxidation of methane in supercritical water by oxygen over a pressure range from 35 to 270 bar and a temperature range from 390 to 440 °C were presented in a paper submitted to the Journal of Physical Chemistry. Raman spectroscopy is used as an *in situ* diagnostic to monitor the concentration of methane, oxygen, carbon monoxide, and carbon dioxide in a constant volume reactor. An existing, high-pressure elementary reaction mechanism reproduces the observed decrease in oxidation rate with increasing pressure and provides insight into the reasons for this behavior. In addition, this quarter Richard Steeper completed requirements for his Ph. D. thesis in the Dept. of Mechanical Engineering at the University of California, Davis.

Methanol oxidation

Work this quarter establishes the quantitative relationship between the experimental results obtained from Sandia's flow reactor experiments and several different elementary chemical kinetics models. A flow diagram was developed, based on elementary reactions, that can describe the important reaction paths present during the oxidation of methanol in supercritical water. In addition, we analyzed the data experimental data to obtain an interpretation of the early reaction

time behavior as an activated process characteristic of a brief induction time. This work is being prepared for submission for journal publication next quarter.

Isopropanol oxidation
Interpretation of results was also the principal activity on this topic during this period. Data obtained last quarter has proven to be sufficient, not only to establish isopropanol oxidation rates, but to identify an induction time and quantify rates of the formation and disappearance of acetone. This work is being prepared for submission for journal publication next quarter.

Hydrogen peroxide thermal decomposition
The flow reactor was tested at reactor conditions and it worked well. Phillip Paul , 8351, who is collaborating with this project on this task, has obtained a cadmium hollow cathode lamp that will provide the probe u.v. source for the experiment. The equipment for this experiment is now in place, but because of other activities in lab that houses the eximer, the start of experiments will be delayed until 9/1/95.

Future work
Work next quarter will focus on completing the propanol oxidation work. We will expand the data set on isopropanol, conduct experiments on n-propanol, and initiate the H_2O_2 experiments. Our present understanding of the initial step in isopropanol oxidation suggests that n-propanol may not behave the same way. The H_2O_2 experiments will provide direct measurement of hydrogen peroxide dissociation rates in supercritical water. The modeling effort will focus on linking the methane and methanol models to the GRI (Gas Research Institute) [1] high temperature model such that we have a self-consistent model with a traceable set of elementary reactions.

Publications & Presentations
S.F. Rice and R.R. Steeper, "Temperature Dependence of the Oxidation of Common Organic Industrial Pollutants in Supercritical Water", submitted to the *Journal of Advanced Oxidation Technologies* , 5/95.

R.R. Steeper, S.F. Rice, Ian M. Kennedy, and J. D. Aiken, "Kinetics Measurements of Methane oxidation in Supercritical Water", submitted to *The Journal of Physical Chemistry*, 6/95.

S.F. Rice, "Kinetic Mechanisms of Supercritical Water Oxidation" presented at The First Annual SERDP Symposium Washington. D.C., 4/95.

D.R. Hardesty, "Kinetic Mechanisms of Supercritical Water Oxidation" presented at the FY95 In Progress Review. 5/95 Ft. Belvoir VA.

R.R. Steeper, "Methane and Methanol Oxidation in Supercritical Water: Chemical Kinetics and Hydrothermal Flame Studies" Ph. D. Dissertation, University of California, Davis. 6/95.

Detailed Summary of Technical Progress this Period

Methane Oxidation (R.R. Steeper)

Much of the work this quarter was on relating the results of our experiments to those reported by Webley et. al. [2] and interpreting the results of the water concentration dependence for the rate of methane oxidation. A non-monotonic dependence of reaction rates on water concentration is observed. With temperature and initial concentrations held constant, methane consumption rates first increase with increasing water concentration but reach a maximum near 5 mol/L. Further increases in water concentration lead to a sharp decrease in the rate of methane consumption. An existing, high-pressure elementary reaction mechanism reproduces this downturn in rates, and provides insight into the reasons for this behavior.

There are several ways that water concentration can affect oxidation rates in supercritical water. First, water is an explicit reactant in many elementary reactions, so that rates of these reactions are directly dependent on water concentration. Second, water is the most important collision partner for unimolecular reactions in the SCWO environment. Unimolecular reaction rates become insensitive to collision partner concentrations at the familiar high-pressure limit, so water's role in these reactions is may have an unusual pressure dependence. A final way that water influences reactions derives from its interaction with transition state complexes: the presence of water can change both the energetics [3] (i. e., which reactions are thermodynamically favored) and the activation volumes (i. e., how reaction rates change as a function of pressure) of these complexes. Results from experiments performed over a range of water concentrations can be used to examine the water concentration dependence of methane oxidation.

Figure 1 compares observed methane concentration histories from a 270-bar and a 135-bar experiment. The two experiments were conducted at approximately the same temperature and initial reactant concentrations. To improve the comparison, time was shifted for both so that a common concentration (well beyond the settling period) was set at time zero. Surprisingly, the data indicate that consumption of methane is faster at the *lower* pressure. The same conclusion is obtained from every pair of 135- and 270-bar experiments that is close enough in initial conditions to be compared. Comparisons can also be made using predictions from the two global rate expressions. With this method, identical initial conditions can be specified, and the results are representative of the entire set of data points. Predictions of the global rate expressions are included in Figure 1: the predictions reinforce the conclusion that rates are significantly faster at 135 bar than at 270 bar. The observed decrease in methane reaction rate with increasing pressure is unexpected. Because of the increase in collision partners with pressure, the primary effect of a pressure increase is to raise reaction rates. The rate of oxidation of phenol in supercritical water has been observed to increase with water density over a range from 6 to 29 mol/L. [4] A similar effect was observed for hydrogen and carbon monoxide over a range of water densities from 1.8 to 4.6 mol/L. [5]

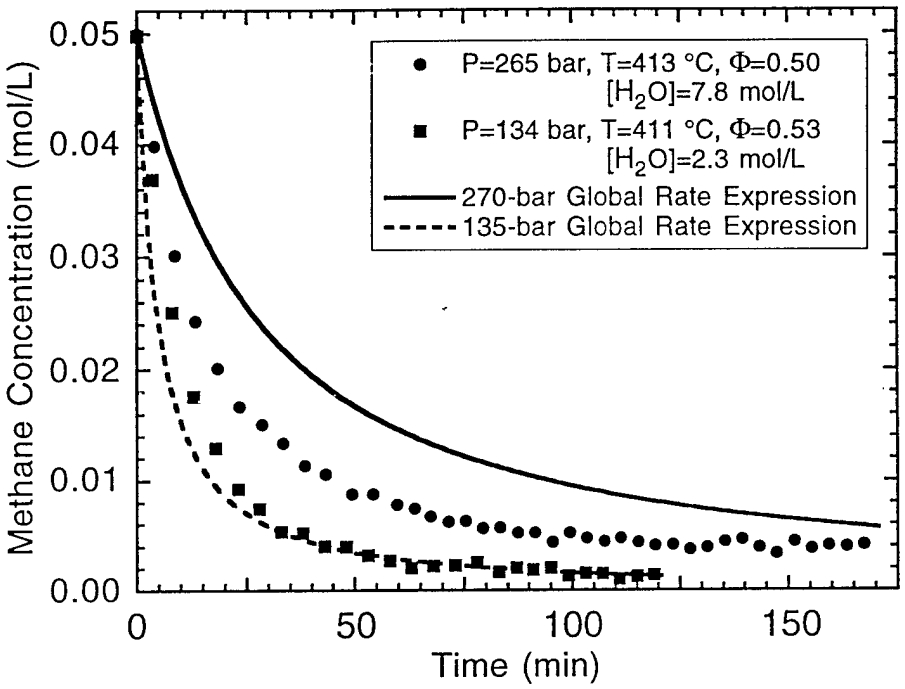

Figure 1. Comparison of methane consumption at 270 and 135 bar. The curves are predictions of the global reaction rate expressions. Note that neither curve is a direct fit to the data in Figure 1; each is calculated using the appropriate set of four constant parameters that represents the data from dozens of experiments. (Φ is the initial fuel equivalence ratio.)

To examine further the observed water concentration dependence, we performed a series of seven experiments. These experiments were conducted at constant initial methane concentration and temperature, while water concentration was varied from 0 to 8 mol/L in the absence of other diluents. The corresponding experimental pressures ranged from 35 to 270 bar. To compare these experimental results, effective rate constants were calculated as described above; they are plotted in Figure 2 as a function of water concentration.

The circles in Figure 2 indicate an initial steady rise in rate constant as water content is increased. However, at a water concentration above 5 mol/L, there is an abrupt downturn in rate. The rate at water concentrations near 8 mol/L has fallen by more than a factor of two from the rate at half that concentration. Included as well in Figure 2 are predictions from the two global rate expressions evaluated at appropriate initial conditions. These two points indicate that the ensemble of 135-bar and 270-bar data supports the observation that rates depend inversely on water content at high water concentrations.

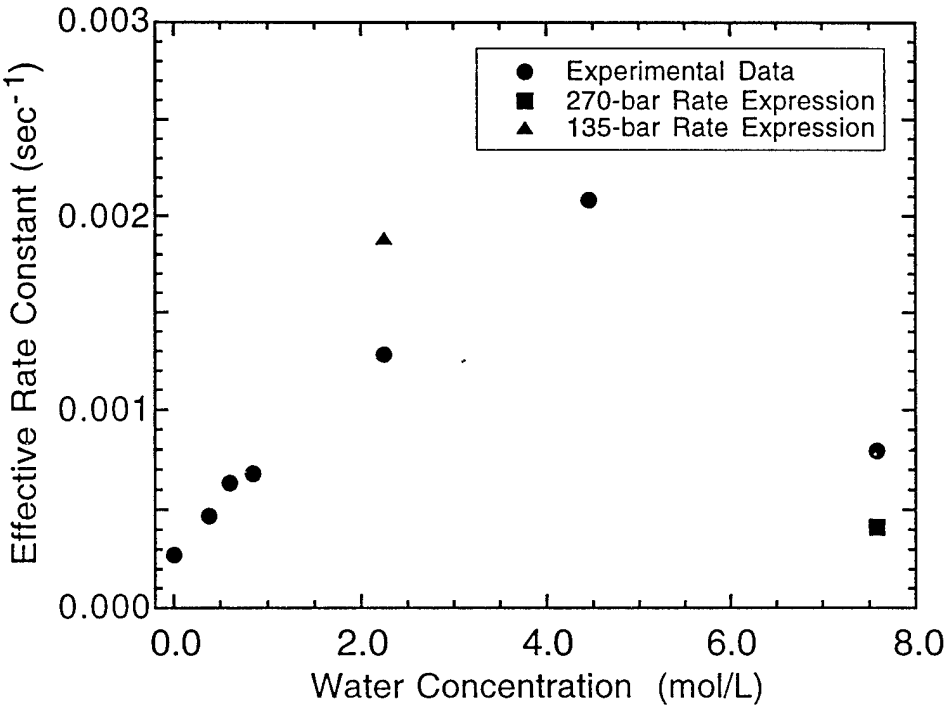

Figure 2. Methane reaction rate constants as a function of water concentration at constant temperature: experimental data and predictions of global reaction rate expressions. For the experimental data, T = 410–413 °C, $[CH_4]_{initial}$ = 0.1–0.15 mol/L, initial fuel equivalence ratio = 0.8–1.0.

To gain insight into the results of our experiments, we tested an elementary reaction mechanism proposed for the oxidation of methanol in supercritical water. [6,7] The mechanism was assembled from a high-pressure H_2-CO mechanism and two atmospheric pressure mechanisms. The rates of key elementary reactions were varied within their uncertainties by the authors to improve agreement with methanol SCWO kinetics experiments performed by . [8] This reaction mechanism was integrated into a constant-temperature, constant-pressure reactor model using Sandia's Chemkin Real Gas package [9]. These constant property assumptions were justified based on the small deviations in temperature and pressure recorded for the abridged data set. Thermodynamic quantities were calculated using a Peng-Robinson equation of state for all species except water, for which an empirical equation of state was used. For this initial assessment of the elementary reaction mechanism, we chose to set all fugacities equal to one in our model.

Figure 3 compares the experimental results with model predictions for the same initial conditions. It is apparent that the model overpredicts the methane consumption rate. Other features of the model predictions however agree with observed trends. For example, the model predicts a negligible induction period for the methane oxidation in agreement with the experiments. Although our experiments are not designed to measure the induction period, the observed data

indicate that this period is a small fraction of the time required to consume the methane. The model predicts a CO maximum concentration equal to approximately 15% of the initial methane load, occurring at a time when about half the methane has been consumed. Results from the 270-bar experiments typically show a smaller CO concentration maximum occurring relatively earlier than predicted by the model. Although not a part of this experimental study, the measured concentration profiles will serve as input into the further development of the SCWO reaction mechanism.

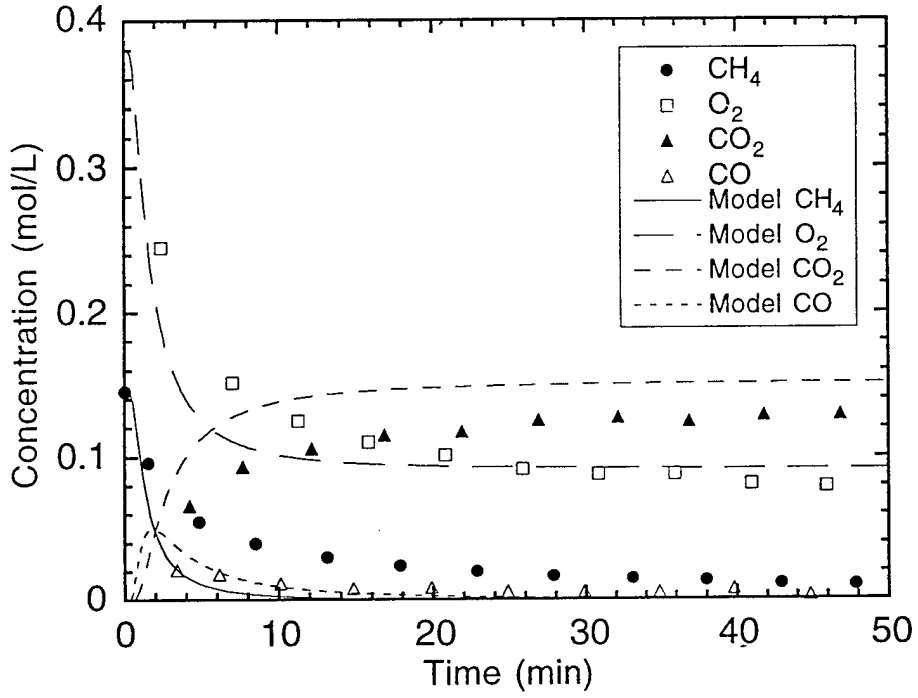

Figure 3. Model predictions of concentration histories compared to observed data.

The elementary reaction mechanism can be used to calculate effective rate constants that help compare model predictions with experimental observations. For example, when calculating rate constants at varying initial methane concentrations, the model predicts a methane reaction order of 1.4, midway between our observed value and that of Webley. Further, the model can be used to predict the rate constant's dependence on water concentration for comparison with the observed dependence. Figure 4 presents such a comparison.

Comparing the predicted and observed data in Figure 4 indicates clearly the overprediction of rates by the model. In assessing the model performance, no attempt was made to improve agreement with experimental data. Since the reaction mechanism in the model was originally optimized using low-

concentration methanol data, it is not surprising that predictions differ from our data. Performing sensitivity and flux analyses, and then tuning the mechanism to our conditions, would likely result in better agreement, albeit at a risk of increasing disagreement with the methanol data.

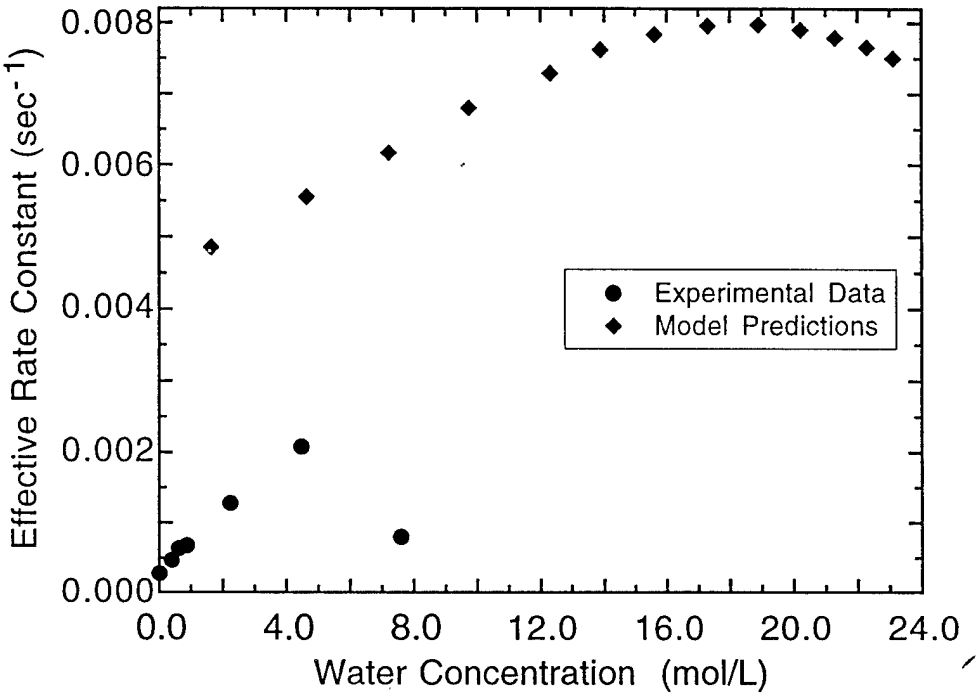

Figure 4. Model predictions of reaction rate constants as a function of water concentration. The experimental data from Figure 5 are included for comparison. Initial conditions for the model predictions are T = 412 °C, $[CH_4]_{initial}$ = 0.05 mol/L, fuel equivalence ratio = 0.5.

Interestingly, despite the discrepancy between the magnitude of measured and predicted rates, Figure 4 shows that the model successfully captures the trend of rates with water concentration that we observe: the model predicts the same abrupt downturn in rates, albeit at a higher water concentration than measured. To understand what causes this downturn, we identified two important reactions from a set of rate-controlling reactions highlighted in earlier studies. [6,10] The first reaction is the unimolecular decomposition of H_2O_2, which is an important chain-branching step:

$$H_2O_2 + M \Rightarrow OH + OH + M. \qquad (2)$$

Increasing the rate of this reaction results in an increased rate of consumption of methane. The other key reaction we identified is the reverse reaction of the CH_3 radical with water to produce CH_4:

$$CH_3 + H_2O = CH_4 + OH. \quad (3)$$

Increasing the rate of Reaction 3 in the direction written slows the overall consumption of methane. Note that water concentration affects the rate of both of these reactions since water is an explicit reactant in Reaction 3, and is the predominant collision partner (represented by M) in Reaction 2.

At low pressures, increasing water concentration increases rates of both elementary reactions linearly. As a result, the difference in rates between Reaction 2 and Reaction 3 grows, and the overall methane consumption rate increases, as seen in the model predictions of Figure 4. At a pressure near 200 bar, however, Reaction 2 reaches its high-pressure limit: at this point it becomes insensitive to the concentration of water. As a result, further increases in water concentration have no effect on Reaction 2. The rate of Reaction 3 continues to increase however, causing the rate of overall methane consumption to fall with increasing water concentration. In support of this simplified hypothesis, we found that increasing the rate of Reaction 3 moved model predictions in the direction of the observed data: overall rates dropped and the location at which rates begin to fall moved to lower water concentrations.

Methanol Oxidation

Work completed last quarter on methanol oxidation showed good agreement between our experimental results and a model developed by Schmitt *et. al.*, [11] This encouraged us to explore further, more subtle, aspects of the oxidation data. In Figure 5, the normalized fuel concentration data (at values less than 0.9) as $\ln([CH_3OH]/[CH_3OH]_o)$ is shown as a function of flow reactor residence time. Here $[CH_3OH]$ refers to the measured methanol concentration and $[CH_3OH]_o$ refers to the initial feed concentration. Assuming that the oxidation proceeds as first–order with respect to fuel, it is possible to linearly extrapolate back to $[CH_3OH]/[CH_3OH]_o=1.0$ and determine the apparent induction time, t_{ind}. It can be seen from Figure 5 that the data are well approximated by first–order kinetics and that all the data sets have a positive intercept revealing a temperature-dependent induction time. Table 1 displays the results of the fit for

$$\frac{[CH_3OH]}{[CH_3OH]_o} = \exp\left(-k_{eff} \cdot (t - t_{ind})\right). \quad (4)$$

Figure 6 shows an Arrhenius plot of both k_{eff} and $(t_{ind})^{-1}$. The parameter k_{eff} is an effective first–order rate constant for the oxidation of methanol after the induction period and $(t_{ind})^{-1}$ is a measurement of the induction period rate constant. The slope of these two curves can be used to determine apparent activation energies for both time periods. The apparent activation energy for the bulk rate constant, k_{eff}, is 179 kJ/mole and for the induction rate constant, $(t_{ind})^{-1}$, is 118 kJ/mole.

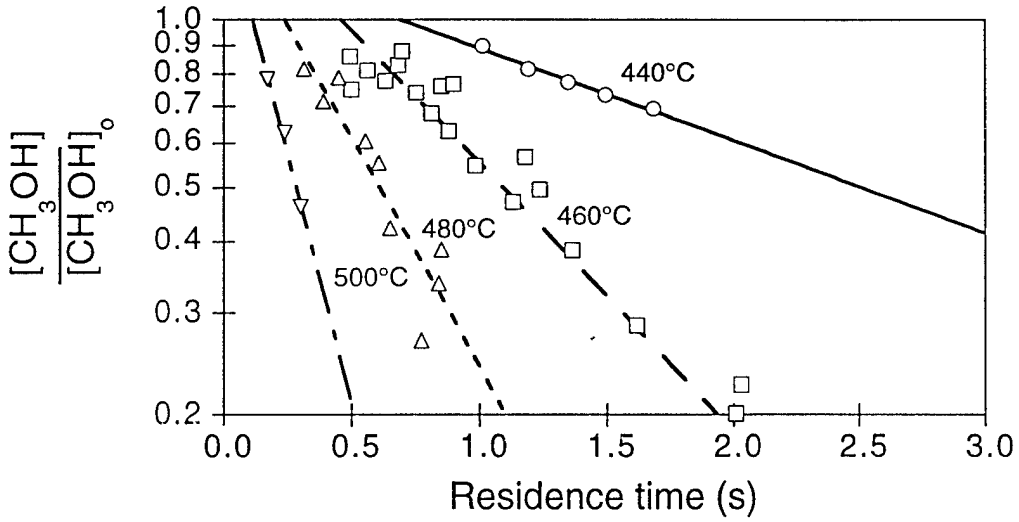

Figure 5. Measured normalized methanol concentrations, normalized by the initial methanol concentration shown as a function of time (data at conversions > 0.1 removed). The lines represent fits of the experimental data to $[CH_3OH]/[CH_3OH]_o = \exp(-k_{eff.}(t-t_{ind}))$ 440°C ○———, 460°C □— — -, 480°C △- - - - -, and 500°C ▽— - -.

Table 1. Parameters from Induction Time Estimate

Temp (°C)	t_{ind} (s)	k_{eff} (s^{-1})
440	0.69	0.38
450	0.55	0.52
460	0.46	1.09
470	0.42	1.63
480	0.24	1.86
490	0.20	2.71
500	0.13	4.05

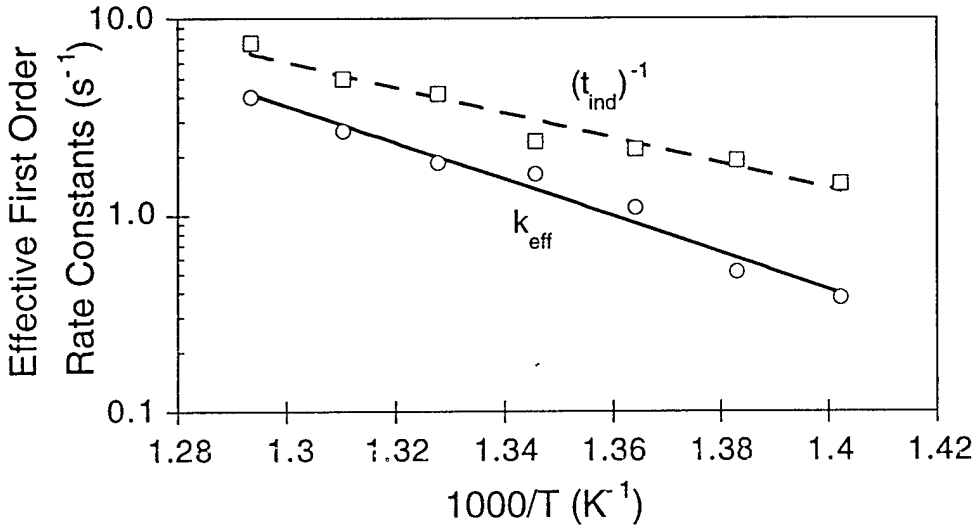

Figure 6. Arrhenius plot of the effective first order rate constant, k_{eff}, and the inverse of the induction time, $(t_{ind})^{-1}$ versus 1000/T. The lines represent least squares fits to the experimental data k_{eff} ○——— and $(t_{ind})^{-1}$ □— — -.

Isopropanol Oxidation (T.B. Hunter)

During this quarter we investigated the oxidation of isopropanol in supercritical water has been investigated using Raman spectroscopy. Results of these experiments for species concentration as a function of residence–time are presented below for temperatures ranging from 400 to 480 °C at constant pressure, 24.4 ± 0.3 MPa, and constant equivalence ratio, 0.88 ± 0.02. Acetone has been identified as the principal intermediate species formed, and subsequently destroyed, during the oxidation process. By assuming first–order kinetics for the destruction of both isopropanol and acetone, effective first–order rate constants have been determined from fits of the experimental data. Assuming Arrhenius behavior, the fits yield rate constants for isopropanol,

$$k_{eff,ipa} = 3.255 \times 10^{22} (s^{-1}) \exp\left[-301.1 (kJ \cdot mol^{-1})/RT\right] \qquad (5)$$

and for acetone,

$$k_{eff,ace} = 1.948 \times 10^{10} (s^{-1}) \exp\left[-137.7 (kJ \cdot mol^{-1})/RT\right]. \qquad (6)$$

These results indicate that, for temperatures greater than 425 °C, the destruction of isopropanol proceeds faster than that of acetone.

One of the main objectives of this work is to obtain data on the supercritical water oxidation of isopropanol that are suitable for kinetic model development and validation. Presented in Table 2 are tabular results of the normalized concentration and residence–time data for isopropanol and acetone, the principal intermediate formed and subsequently destroyed during the oxidation. Normalized concentrations are defined as the measured species concentration, i.e., isopropanol, [ipa], or acetone, [ace], divided by the initial isopropanol concentration, $[ipa]_o$.

Table 2 Experimental Measurements of Normalized Isopropanol and Acetone Concentrations [a]

Run 1, T = 400 °C			Run 2, T = 409 °C			Run 3, T = 420 °C		
t (s)	$\frac{[ipa]}{[ipa]_o}$	$\frac{[ace]}{[ipa]_o}$	t (s)	$\frac{[ipa]}{[ipa]_o}$	$\frac{[ace]}{[ipa]_o}$	t (s)	$\frac{[ipa]}{[ipa]_o}$	$\frac{[ace]}{[ipa]_o}$
0.79	0.98	0.02	0.72	0.95	0.03	0.63	0.92	0.06
1.07	0.87	0.04	0.97	0.92	0.03	0.92	0.93	0.12
1.41	0.82	0.08	1.27	0.88	0.10	1.20	0.79	0.18
1.82	0.76	0.08	1.60	0.87	0.13	1.43	0.72	0.22
2.02	0.82	0.09	1.90	0.80	0.11	1.68	0.48	0.32
2.41	0.77	0.11	2.23	0.66	0.21	2.00	0.32	0.39
Run 4, T = 430 °C			**Run 5, T = 440 °C**			**Run 6, T = 450 °C**		
t (s)	$\frac{[ipa]}{[ipa]_o}$	$\frac{[ace]}{[ipa]_o}$	t (s)	$\frac{[ipa]}{[ipa]_o}$	$\frac{[ace]}{[ipa]_o}$	t (s)	$\frac{[ipa]}{[ipa]_o}$	$\frac{[ace]}{[ipa]_o}$
0.58	0.84	0.03	0.58	0.84	0.24	0.56	0.71	0.19
0.82	0.82	0.13	0.77	0.72	0.27	0.73	0.44	0.33
1.09	0.51	0.22	1.03	0.30	0.44	0.97	0.09	0.40
1.36	0.26	0.31	1.26	0.07	0.47	1.21	0.00	0.33
1.55	0.07	0.40	1.47	0.01	0.42	1.34	0.00	0.27
1.85	0.00	0.40	1.70	0.02	0.34	1.62	0.01	0.15
Run 7, T = 460 °C			**Run 8, T = 470 °C**			**Run 9, T = 480 °C**		
t (s)	$\frac{[ipa]}{[ipa]_o}$	$\frac{[ace]}{[ipa]_o}$	t (s)	$\frac{[ipa]}{[ipa]_o}$	$\frac{[ace]}{[ipa]_o}$	t (s)	$\frac{[ipa]}{[ipa]_o}$	$\frac{[ace]}{[ipa]_o}$
0.52	0.56	0.41	0.49	0.23	0.42	0.48	0.06	0.28
0.71	0.11	0.40	0.68	0.02	0.43	0.64	0.00	0.19
0.94	0.04	0.37	0.90	0.00	0.25	0.87	0.00	0.08
1.17	0.00	0.22	1.11	0.02	0.12	1.11	0.02	0.04
1.34	0.00	0.16	1.29	0.02	0.12	1.27	0.00	0.01
1.55	0.02	0.10	1.53	0.02	0.07	1.48	0.02	0.03

[a] t (s) = residence time (s), $\frac{[ipa]}{[ipa]_o} = \frac{\text{isopropanol concentration}}{\text{isopropanol concentration}_{initial}}$, $\frac{[ace]}{[ipa]_o} = \frac{\text{acetone concentration}}{\text{isopropanol concentration}_{initial}}$.

In Figure 7, the results for experiments 2, 4, 6, and 8 are shown. It is apparent from Figure 7, as expected, that the isopropanol disappearance rate increases with increasing temperature. This, in turn, directly impacts the production rate of acetone, which also increases with increasing temperature.

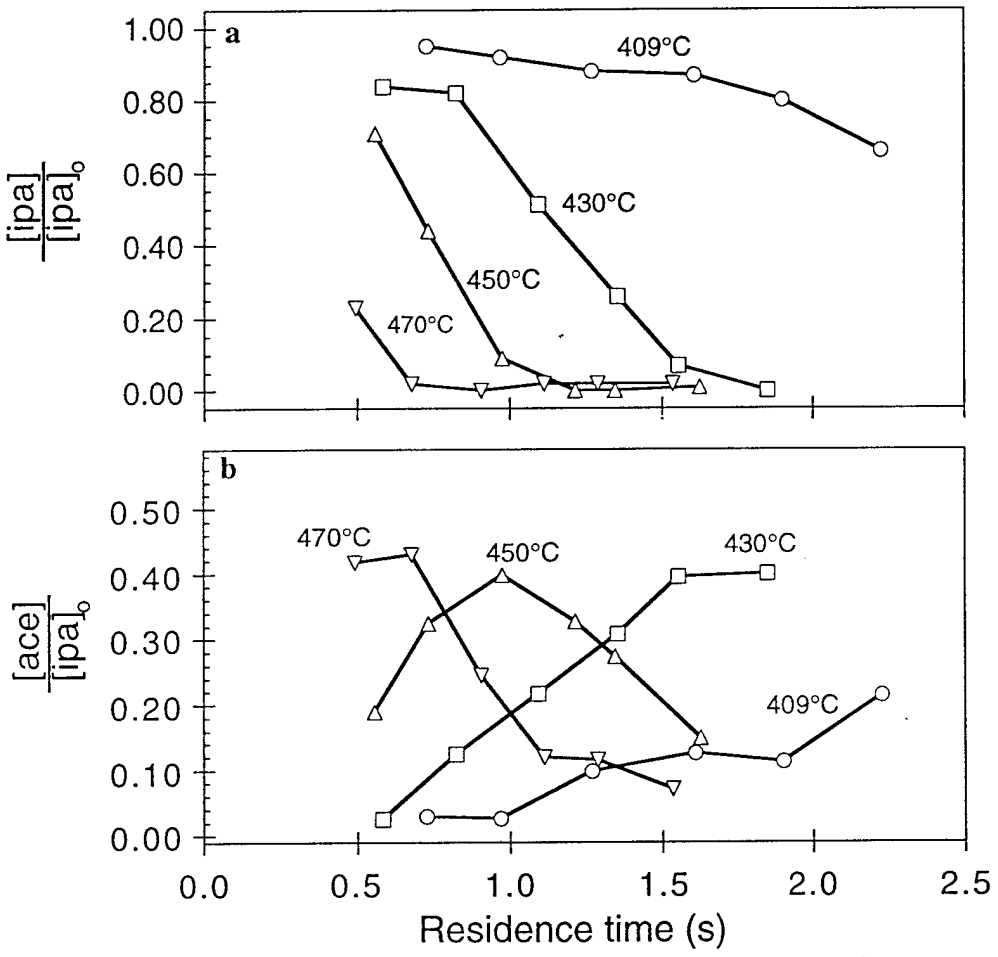

Figure 7. Measured normalized species concentration profiles plotted versus residence–time for (a) isopropanol and (b) acetone, runs 2 (409°C)○, 4 (430°C)□, 6 (450°C)△, and 8 (470°C)▽.

Despite the current lack of a detailed kinetic model to more thoroughly explore these data, it is possible to gain considerable insight through global kinetic analysis. Such models represent a consolidation of more complex reaction schemes and permit an initial indication of species reactivity. For the current analysis, first–order kinetics is assumed for the destruction of both isopropanol and acetone. This type of analysis has been used in the reduction of SCWO data in the past and has been found to provide a reasonable representation of the experimental data.

When the destruction of isopropanol is assumed to be first–order with respect to fuel and zeroth–order with respect to oxygen, the following equation is obtained

$$\frac{d[ipa]}{dt} = -k_{eff,ipa}[ipa] \qquad (7)$$

where $k_{eff,\ ipa}$ is the effective first–order rate constant. For each experiment in which sufficient data was acquired (i.e., at least two points, runs 1 through 7), a linear, least squares fit was performed on the natural logarithm of normalized isopropanol concentration versus residence–time data. The slope of this fit gives $k_{eff,\ ipa}$ and the intercept at a normalized isopropanol concentration of unity corresponds to the apparent induction time, t_{ind}. If it is assumed that $k_{eff,\ ipa}$ has an Arrhenius behavior, then both the preexponential, A, and the activation energy, E_a, can be calculated by performing a linear fit of $\ln(k_{eff,\ ipa})$ versus 1/T, see Figure 8. The analysis gives $E_{a,\ ipa} = 301.1$ kJ·mol^{-1} and $A_{ipa} = 3.255 \times 10^{22}$ s^{-1}.

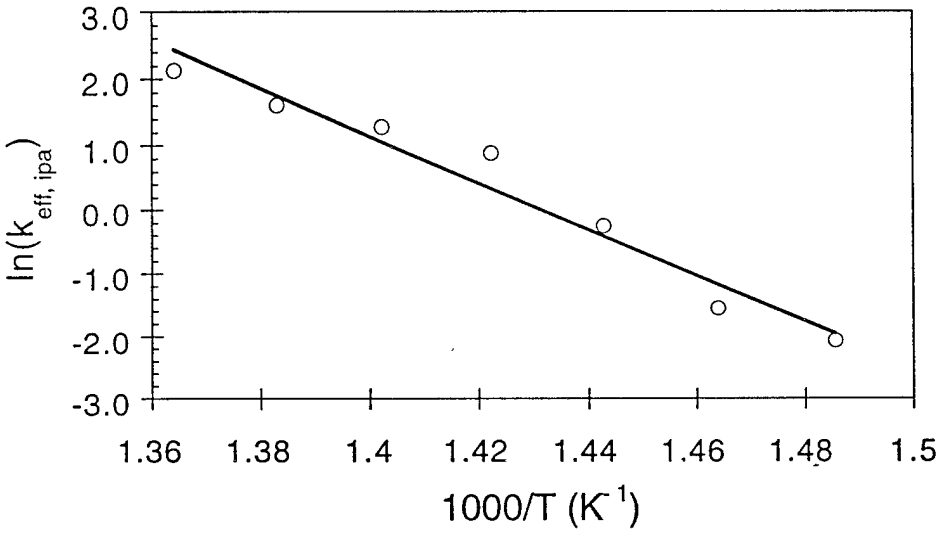

Figure 8. Effective first order rate constants for isopropanol destruction (runs 1-7) plotted versus 1000/T (the line is calculated from a linear least squares fit of the data).

The experimental results for isopropanol indicate that there is a temperature dependent induction time, t_{ind}, i.e., a time after entry of the reactant mixture into the flow reactor during which, little to no reaction occurs. Therefore, to compare the calculated first–order kinetic results to the experimental data it is necessary to calculate or estimate t_{ind} for each of the data sets. The induction time was determined for runs 3–7 by extrapolation to a normalized isopropanol concentration of unity, as previously discussed. It is apparent that t_{ind}, for runs 3–7, is roughly linearly dependent on temperature, see Figure 9. For runs 1 and 2 the change in the concentration of isopropanol is sufficiently small that noise in the measurement results in induction times that are unreasonable. For runs 8 and 9 there is not

sufficient data to extrapolate the concentration measurements. Therefore, the linear fit was used to approximate the induction times for runs 1, 2, 8, and 9.

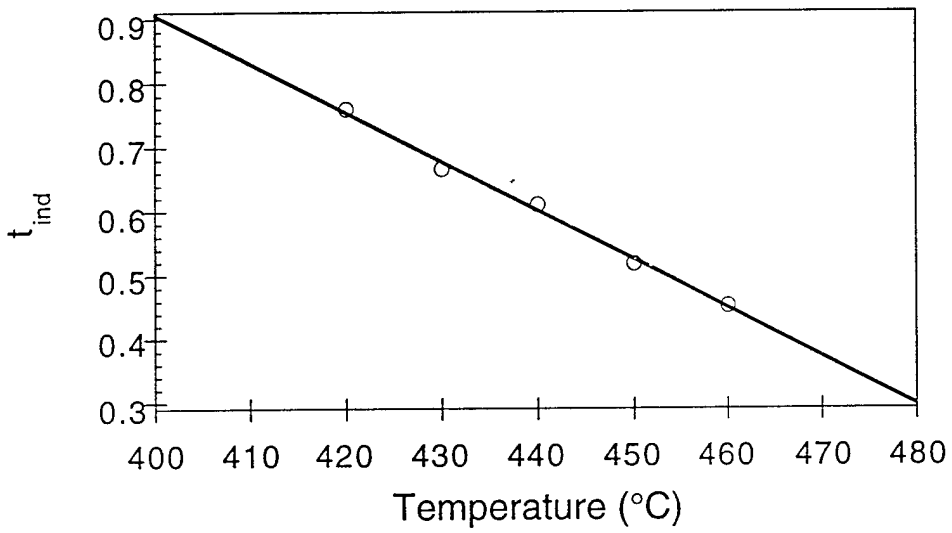

Figure 9. Measured induction times for isopropanol destruction (runs 3-7) plotted versus temperature (the line is calculated from a linear least squares fit of the data).

To compare the first–order model to the experimental data, Equation 7 must be integrated from $[ipa]_o$ to [ipa] for isopropanol concentration and from t_{ind} to t for residence time to obtain

$$\frac{[ipa]}{[ipa]_o} = \exp\left(-k_{eff,ipa} \cdot \left(t - t_{ind}\right)\right) \quad \text{for } t \geq t_{ind}. \tag{8}$$

For residence times less than the induction time the normalized concentration is set to unity. The model and experimental results are plotted in Figure 10. It is apparent that first–order kinetics reproduce the experimental data reasonably well.

Since acetone is simultaneously produced and destroyed during the isopropanol oxidation process, examining its destruction rate is more difficult. If, however, it is possible to extract concentration data where the production rate is sufficiently small, then the destruction rate can be effectively determined. For the current analysis it is assumed that normalized isopropanol concentrations below 10% of the original value are acceptably small. In Figure 11, the normalized acetone concentration is plotted versus residence time for conditions meeting the above criterion, i.e., $[ipa]/[ipa]_o < 0.1$. This plot indicates that, as for isopropanol, the disappearance rate of acetone increases with increasing temperature.

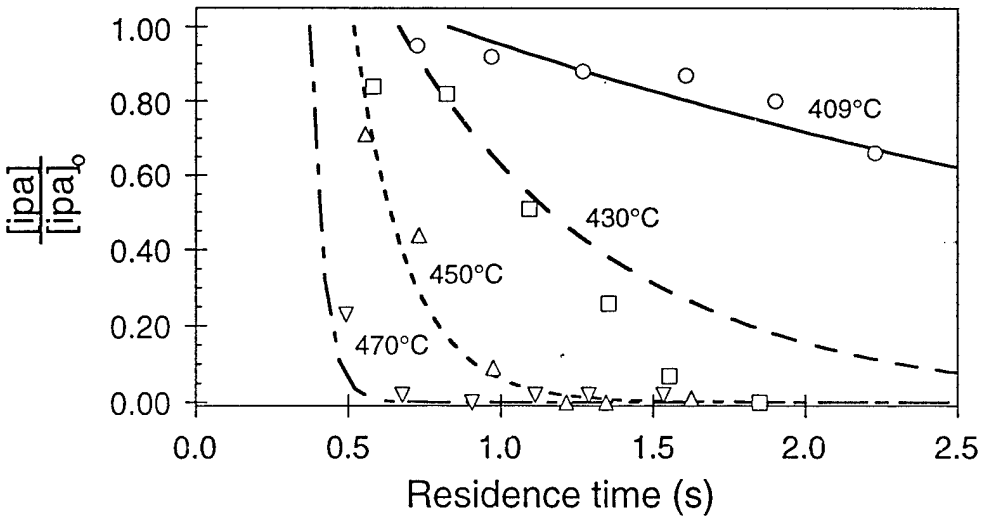

Figure 10. Comparison of calculated first order reaction kinetics (lines) to isopropanol experimental data (open symbols) for runs 2 (409°C)○———, 4 (430°C)□— — -, 6 (450°C)△- - - - -, and 8 (470°C)▽— - -.

Using this bounded acetone data set, i.e., acetone concentrations when $[ipa]/[ipa]_o < 0.1$, it is possible to obtain an effective first–order rate constant for the destruction of acetone by following a method similar to that used for determining the effective rate for isopropanol. If it is assumed that the destruction rate of acetone is first–order with respect to acetone and zeroth–order with respect to oxygen, then an effective first–order rate constant, $k_{eff,\,ace}$, can be determined for the data shown in Figure 11. If it is assumed that $k_{eff,\,ace}$ has Arrhenius dependence, then both the preexponential factor and the activation energy can be calculated by performing a linear least squares fit of $\ln(k_{eff,\,ace})$ versus $1/T$. This analysis gives $E_{a,\,ace} = 85.12$ kJ·mol^{-1} and $A_{ace} = 2.233 \times 10^6$ s^{-1}. While this analysis is reasonable, it only allows the use of a small fraction of the experimental data. With an additional assumption regarding the production of acetone, a more rigorous analysis can be performed allowing all of the experimental data to be used in the fit of $k_{eff,\,ace}$.

If it is assumed that all of the isopropanol that is destroyed proceeds through the acetone channel, then the destruction rate of isopropanol is equal to the production rate of acetone. If we again assume that the destruction of acetone is first–order with respect to acetone and zeroth–order with respect to oxygen, it is possible to write the following equation for the total rate of change of the acetone concentration

$$\frac{d[ace]}{dt} = k_{eff,ipa}[ipa] - k_{eff,ace}[ace]. \qquad (9)$$

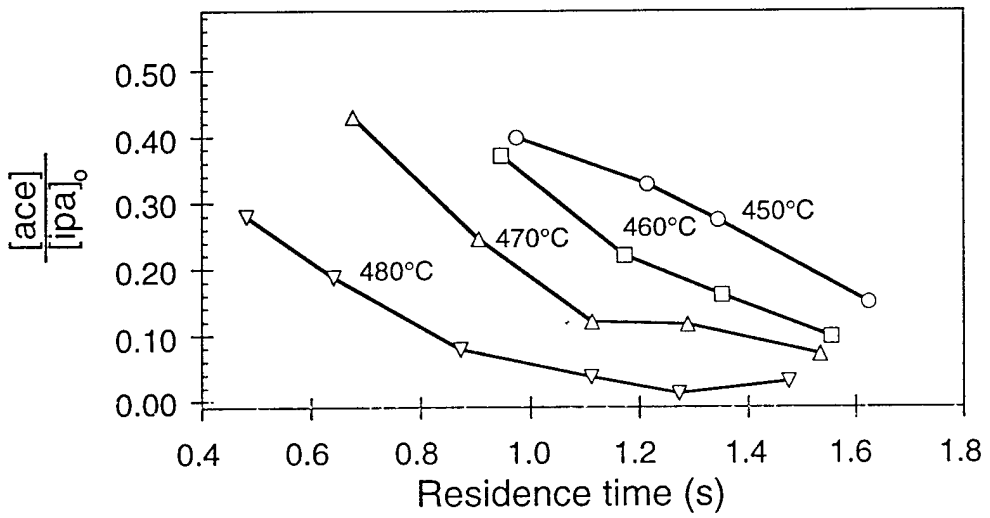

Figure 11. Measured acetone concentration plotted versus residence–time for conditions when the normalized isopropanol concentration is less than 0.1, runs 6 (450°C) ○, 7 (460°C) □, 8 (470°C) △, and 9 (480°C) ▽.

Equation 9 can be integrated analytically (given the boundary condition [ace] at t = t_{ind} is equal to 0) to give the following equation for the evolution of acetone

$$\frac{[ace]}{[iso]_o} = \frac{k_{eff,ipa}}{k_{eff,ace} - k_{eff,ipa}} \left\{ \exp\left[-k_{eff,ipa} \cdot (t - t_{ind})\right] - \exp\left[-k_{eff,ace} \cdot (t - t_{ind})\right] \right\} \quad \text{for } t \geq t_{ind}. \quad (10)$$

The only unknown in this equation is $k_{eff,\ ace}$, which, if Arrhenius behavior is assumed, is dependent on A_{ace} and $E_{a,\ ace}$. Using our experimental data, these parameters were determined by minimizing the square of the error between the predicted and the observed value of the normalized acetone concentration, giving $E_{a,\ ace}$ = 137.7 kJ·mol^{-1} and $A_{ace} = 1.948 \times 10^{10}$ s^{-1}. In this analysis we have assumed that during the induction time little to no reaction of isopropanol occurs, therefore, we have also assumed that no acetone is formed during the induction time, i.e., for residence times less than the induction time the concentration of acetone is zero.

Using these parameters for $E_{a,\ ace}$ and A_{ace} and the previously determined values of t_{ind} and $k_{eff,\ ipa}$, the normalized concentration of acetone can be calculated with equation 10. These results are plotted along with the experimental data in Figure 12. It is again evident that even with this rudimentary model for the oxidation of isopropanol and acetone, first–order kinetics (with an induction time) does a reasonable job of approximating the production and destruction of acetone in this system.

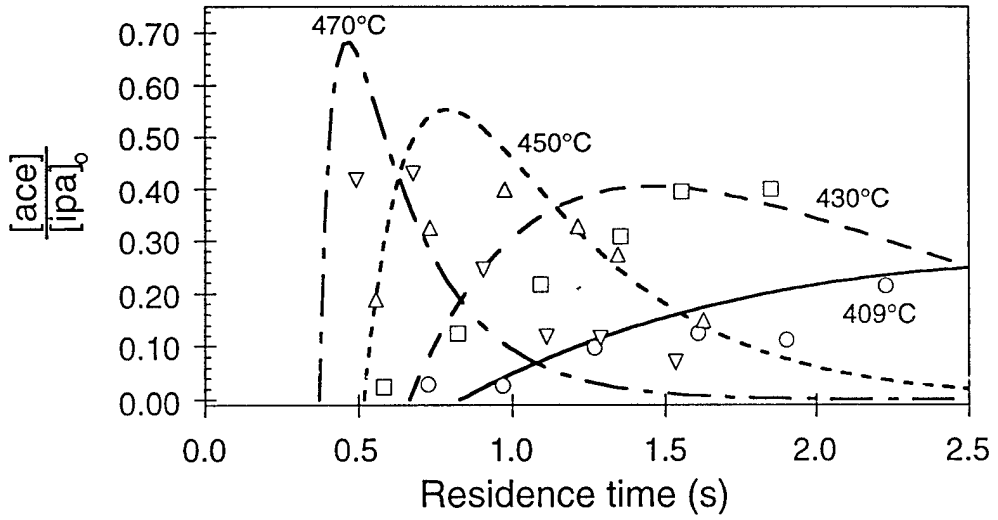

Figure 12. Comparison of calculated first order reaction kinetics (lines), to acetone experimental data (open symbols) for runs 2 (409°C)○———, 4 (430°C)□— — -, 6 (450°C)△- - - - -, and 8 (470°C)▽— - -.

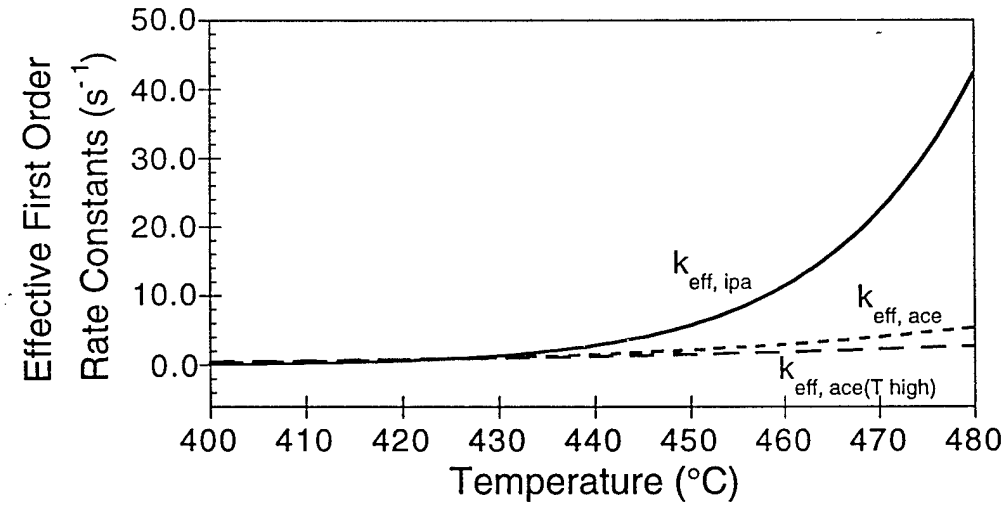

Figure 13. Comparison of the calculated effective first order rate constants for the oxidation of isopropanol, $k_{eff,\ ipa}$———, and acetone (using two different fitting methods) $k_{eff,\ ace}$- - - - - and $k_{eff,\ ace(T\ high)}$— — -.

Finally, it is interesting to compare the two calculated first–order rate constants for acetone oxidation and to compare these constants to that determined for isopropanol. In Figure 13 the three rate constants are shown over the temperature range of the current work. In the figure, $k_{eff,\ ace(T\ high)}$ represents the rate constant calculated based on the first method discussed, i.e., using the constrained ($[ipa]/[ipa]_o < 0.1$), high temperature acetone results. This rate constant compares quite favorably to the rate constant determined using the full acetone data set, represented by $k_{eff,\ ace}$. While the second method requires an additional assumption, it allows a more thorough fit, using all of the experimental acetone concentration data. Both rate constants intersect the isopropanol rate constant at ~425 °C. Below 425 °C $k_{eff.\ ace(T\ high)} > k_{eff,\ ace}$; however, their maximum deviation is less than a factor of 1.4. Above 425 °C $k_{eff,\ ace} > k_{eff.\ ace(T\ high)}$; the maximum deviation is again small, less than a factor of 2. The current results indicate that for temperatures above 425 °C and pressures of approximately 24.4 MPa acetone is more difficult to oxidize than isopropanol, while below 425 °C the opposite is true. Preliminary results from our lab for temperatures extending into the subcritical temperature region (350–400 °C) support the observation that the acetone destruction rate is faster than that of isopropanol for lower temperatures.

Plans for next quarter

Experimental emphasis will be placed on completing the data set for isopropanol oxidation along with the quantification of the rate of formation of CO, and perhaps CO_2, in this system. We will also examine the rate of consumption of O_2. When this information is combined, we will be able to estimate the rate of heat release. This is the critical engineering design information needed to evaluate the practicalities of using isopropanol as a make-up fuel in SCWO reactors. We will also conduct experiments on n-propanol to compare intermediates and rate of heat release for this isomeric molecule with a nearly identical heat of formation that cannot form acetone . Other experimental work will focus on the H_2O_2 experiments described above.

Our approach will be focused on joining the methane model and the methanol model that we have used up to this point and reconciling them with a high pressure version of the well -documented GRI mechanism. We will then use this C1 system as a basis for development of the fundamental mechanisms the larger organic molecules.

References

1. Frenklach, M., Wang, H., Bowman, C. T., Hanson, R. K., Smith, G. P., Golden, D. M., Gardiner, W. C., and Lissianski, V., An Optimized Kinetic Model for Natural Gas Combustion, Poster session, Twenty-Fifth Symposium (International) on Combustion, The Combustion Institute, Pittsburgh, PA, 1994 (additional

information on the GRI project and mechanisms can be obtained from the WWW site, http://diesel.fsc.psu.edu/~gri_mech or from the FTP site, vax.sri.com).

2. Webley, P. A.; Tester, J. W. *Energy & Fuels* **1991**, *5*, 411.

3. Melius, C. F.; Bergan, N. E. "Effects of Water on Combustion Kinetics at High Pressure"; Twenty-Third Symposium (International) on Combustion, 1990.

4. Thornton, T. D.; Savage, P. E. *AIChE Journal* **1992**, *38*, 321.

5. Holgate, H. R.; Tester, J. W. *J. Phys. Chem.* **1994**, *98*, 800.

6. Alkam, M. K.; Butler, P. B.; Pitz, W. J. "Methanol and Hydrogen Oxidation Kinetics in Water at Supercritical States," Report No. UIME PBB 95-001, University of Iowa, 1995.

7. Alkam, M. K.; Pai, V. M.; Butler, P. B.; Pitz, W. J. Submitted to *Combustion and Flame* **1995**.

8. Webley, P. A.; Tester, J. W.; Holgate, H. R. *Ind. Eng. Chem. Res.* **1991**, *30*, 1745.

9. Schmitt, R. G.; Butler, P. B.; French, N. B. "CHEMKIN Real Gas: A FORTRAN Package for Analysis of Thermodynamic Properties and Chemical Kinetics in Nonideal Systems," University of Iowa, Report No. UIME PBB 93-006, 1993.

10. Holgate, H. R.; Tester, J. W. *J. Phys. Chem.* **1994**, *98*, 810.

11. Schmitt, R. G.; Butler, P. B.; Bergan, N. E.; Pitz, W. J.; Westbrook, C. K. Destruction of Hazardous Waste in Supercritical Water. Part II: A Study of High-Pressure Methanol Oxidation Kinetics. 1991 Fall Meeting of the Western States Section/The Combustion Institute, University of California at Los Angeles, CA, 1991, 19.

Dr. E. Fenton Carey, Jr.
U.S. Department of Energy (ST-60)
1000 Independence Avenue, S.W.
Room GA 155
Washington, DC 20585

Dr. Robert Marianelli
U.S. Dept. Of Energy
19901 Germantown Rd.
Germantown, MD 20874

Jim Hurley
US AF AL/EQS
139 Barnes Drive, Suite 2
Tyndall Air Force Base, FL 32403

Dr. Peter Schmidt
Office of Naval Research
Chemistry Division
800 North Quincy Street
Arlington, VA 22217-5660

Dr. Robert Shaw
Chemical & Biological Sciences Div.
U.S. Army Research Office
Research Triangle Park, NC 27709-2211

Prof. Martin A. Abraham
The University of Tulsa
Department of Chemical Engineering
600 South College Avenue
Tulsa, OK 74104-3189

Prof. Joan F. Brennecke
University of Notre Dame
Department of Chemical Engineering
Notre Dame, IN 46556

Dr. Kenneth Brezinsky
Dept. of Mechanical and Aerospace Engineering
Princeton University
PO Box CN5263
Princeton, NJ 08544-5263

Prof. Klaus Ebert
Kernforschungszentrum Karlsruhe
Institut fur Heisse Chemie
Postfach 3640
D-76021 Karlsruhe
Germany

Prof. Earnest F. Gloyna
University of Texas at Austin
Environmental and Health Engineering
Austin, TX 78712

Prof. Phillip E. Savage
University of Michigan
Chemical Engineering Department
Herbert H. Dow Building
Ann Arbor, MI 48109-2136

Carl Adema
SERDP Program Office
Program Manager for Compliance and Global Environmental Change
901 North Stuart Street, Suite 303
Arlington, VA 22203

Trienel Ahearn.
Labat-Anderson Incorporated
8000 Westpark Dr.
Suite 400
McLean, VA 22102

K.S. Ahluwalia
Foster Wheeler Development Corporation
Engineering Science & Technology
12 Peach Tree Hill Road
Livingston, NJ 07039

Dr. Steven J. Buelow
CST-6
Los Alamos National Lab.
Los Alamos, NM 87545

Ernest L. Daman
Foster Wheeler Development Corporation
12 Peach Tree Hill Road
Livingston, NJ 07039

Philip C. Dell'Orco
Los Alamos National Laboratory
Explosives Technology & Safety C920
Los Alamos, NM 87545

John Harrison
SERDP Program Office
901 North Stuart Street, Suite 303
Arlington, VA 22203

Dr. David A. Hazelbeck
General Atomics
M/S 15-100D
3550 General Atomics Court
San Diego, CA 92121-1194

Dr. Glenn T. Hong
MODAR, Inc.
14 Tech Circle
Natick, MA 01760

W. Killilea
MODAR, Inc.
14 Tech Circle
Natick, MA 01760

Richard Kirts
Naval Civil Engineering Laboratory
560 Laboratory Dr.
Port Hueneme, CA 93043-4328

Richard C. Lyon
Eco Waste Technologies
2305 Donley Drive
Suite 108
Austin, TX 78758-4535

Dr. Michael Modell
Modell Environmental Corporation
300 5th Avenue, 4th Floor
Waltham, MA 02154

Prof. Jean Robert Richard
CNRS
Combustion Laboratory
1C Avenue de la Recherche Scient.
Orleans 45071
France

Crane Robinson
Arament Reseasrch
Development & Engineering Center (ARDEC)
SMCAR-AES-P
Building 321
Picatinny Arsenal, NJ 07806-5000

Dr. Gregory J. Rosasco
Nat'l Institute of Standards and Technology
Division 836, Bldg. 221, Rm B-312
Gaithersburgh, MD 20899

Prof. Jefferson W. Tester
Massachusetts Institute of Technology
Energy Laboratory
Room E40-455
77 Massachusetts Avenue
Cambridge, MA 02139

Phil Whiting
Abitibi-Price Inc.
2240 Speakman Drive
Mississauga, Ontario L5K 1A9
Canada

Marvin F. Young
Aerojet
PO Box 13222
Sacramento, CA 95813-6000

MS0756 G.C Allen, 6607

MS9001 T.O. Hunter, 8000
Attn: D.L. Crawford, 1900
E.E. Ives, 5200
M.E. John, 8100
L.A. West, 8600
R.C. Wayne, 8700

MS9054 W.J. McLean, 8300

MS9051 L. Rahn, 8351

MS9055 F. Tully, 8353

MS9056 G. Fisk, 8355

MS9052 D.R. Hardesty, 8361
Attn: Allendorf, S
Allendorf, M
Baxter, L

MS9052 J. Aiken, 8361

MS9052 R. Hanush, 8361

MS9052 T. Hunter, 8361

MS9052 S. Rice, 8361

MS9053 R. Steeper, 8362

MS9053 R. Carling, 8362

MS9053 C. Hartwig, 8366

MS9105 L.A. Hiles, 8400

MS9406 B. Haroldsen, 8412

MS9406 H. Hirano, 8412

MS9406 C. LaJeunesse, 8412

MS9406 M.C. Stoddard, 8412

MS9404 B. Mills, 8713